https://doi.org/10.5194/egusphere-2026-2808
Preprint. Discussion started: 11 June 2026

Climate-sensitive Derived Flood Frequency Analysis Based on Flood Events Characteristics

Luigi Cafiero[1], Miriam Bertola[2], Peter Valent[2,4], Francesco Laio[1], Günter Blöschl[2,3], and Alberto Viglione[1]

[1]Department of Environment, Land and Infrastructure Engineering, Politecnico di Torino, Corso Duca degli Abruzzi, 24, Turin, 10129, Italy
[2]Institute of Hydraulic Engineering and Water Resources Management, Vienna University of Technology, Karlsplatz 13/222, Vienna, 1040, Austria
[3]Department of Civil, Chemical, Environmental, and Materials Engineering, Università di Bologna, Viale del Risorgimento, 2, Bologna, 40136, Italy
[4]Department of Land and Water Resources Management, Slovak University of Technology, Radlinského 2766/11, 810 05 Bratislava, Slovakia

Correspondence: Luigi Cafiero (luigi.cafiero@polito.it)

Abstract. Understanding how flood frequency changes under non-stationary hydro-climatic conditions remains a key challenge in hydrology. This study presents a Bayesian process-based framework for flood frequency analysis that explicitly accounts for the seasonal dependence of rainfall–runoff processes and their sensitivity to climate change. The approach links an event-based rainfall–runoff model with probabilistic representations of storm, soil moisture, and catchment response, allowing the joint propagation of uncertainty from climate drivers to flood quantiles. The process-based structure of the framework also enables the disentangling of individual flood drivers, such as the upward shift of the zero-degree isotherm, long-term changes in soil moisture regimes, and variations in precipitation intensity. The framework is implemented in Austrian hotspots, i.e. groups of similar catchments, using long-term hydrometeorological records and regional climate projections (EURO-CORDEX). Results show that (i) changes in flood frequency are primarily driven by projected increases in precipitation intensity, while temperature and soil moisture act as modulators or amplifiers of this signal; (ii) precipitation changes have larger but more uncertain impacts on floods than temperature and soil moisture variations; (iii) the expected reduction in soil moisture tends to mitigate frequent floods but has mores limited influence on rare events. The proposed methodology provides a transferable tool for assessing climate-sensitive flood hazards in non-stationary environments.

1 Introduction

Floods are among the most damaging natural hazards worldwide, and their frequency and magnitude are undergoing substantial modification under changing hydroclimatic conditions. Several studies have documented significant shifts in flood regimes across Europe and globally, driven by changes in precipitation, snowmelt, and soil moisture dynamics (Blöschl et al., 2019). The European Floods Directive (2007/60/EC) explicitly recognizes the need to account for climate change in flood risk assessment, while the Intergovernmental Panel on Climate Change (IPCC) emphasizes that intensification of the hydrological cycle

https://doi.org/10.5194/egusphere-2026-2808
Preprint. Discussion started: 11 June 2026

will likely alter the frequency and severity of floods in many regions (Camici et al., 2014). Recent evidence from Austria shows marked increases in both daily and hourly heavy rainfall over the past four decades, about 8% and 15%, respectively, consistent with Clausius–Clapeyron scaling and regional temperature increases (Haslinger et al., 2025). However, the link between precipitation change and flood change is not straightforward. While daily heavy rainfall changes are consistent with flood increase in large catchments, flood increases in small catchments (25% over the last four decades) are stronger than hourly rainfall changes (Haslinger et al., 2025). Moreover, while Westra et al. (2014) found that short-duration rainfall extremes have intensified across much of Europe, flood magnitude trends remain spatially heterogeneous, suggesting the concurrent influence of multiple controlling factors.

In addition to precipitation, another main factor modulating the rainfall–flood relationship is the antecedent catchment condition. Soil moisture and storage state determine how rainfall is partitioned between infiltration and direct runoff, and thus strongly influence the flood response (Merz and Blöschl, 2003). Numerous studies have shown that antecedent wetness plays a dominant role in shaping flood volume, particularly for smaller and more frequent floods, while for large, rare floods, precipitation intensity tends to prevail (Bennett et al., 2018; Wasko et al., 2021; Ho et al., 2023). This dual control implies that both precipitation and antecedent conditions must be jointly considered to understand and predict flood regime changes. Antecedent catchment conditions are reflected in the event runoff coefficient which represents the share of precipitation directly contributing to the runoff. A general decrease of runoff coefficients is expected with increasing temperatures meaning that possible rainfall increases may be offset by drier soils. Moreover, Wasko et al. (2021) found that an increase in variability of runoff coefficients is expected across most locations, resulting in increased variability in floods. Runoff coefficient also vary at event-scale according to different precipitation characteristics. Merz and Blöschl (2003) found that runoff coefficients tend to increase with rainfall depth for long-rain floods, while it exhibit a larger scatter for flash floods (saturation vs infiltration excess runoff generation mechanism).

Snow storage and snowmelt also play a crucial role in modulating flood response, particularly in temperate and cold regions. In snowmelt-dominated or mixed rain–snow regimes, flood generation is strongly influenced by the timing and energy available for melt, which constrains the upper tail of the flood frequency curve (Merz and Blöschl, 2003, 2008). Observed reductions in snow cover extent and earlier melt peaks across the Northern Hemisphere (Estilow et al., 2015; Madsen et al., 2014) indicate that warming temperatures are already altering snow-driven flood regimes. The hydrological effects of these changes depend on regional flood seasonality and the mixing of flood-generating processes. For instance, snowmelt changes mainly affect small spring floods in southern Alpine catchments, but can influence the entire flood frequency curve in northern Europe (Merz and Blöschl, 2003; Kemter et al., 2020). Recent attribution studies highlight the importance of changes in precipitation, soil moisture and snowmelt in shaping flood regime shifts across Europe (Bertola et al., 2021), pointing to the need for a process-based understanding of how different flood generation mechanisms respond to climate forcing.

Given these complexities, a wide range of methods has been developed for estimating design floods. These can broadly be classified into (a) statistical, (b) deterministic, and (c) hybrid or derived approaches (Rogger et al., 2012; Hall et al., 2014; Winter et al., 2019). Statistical methods fit probability distributions to observed peak flows and provide robust estimates when long, stationary records exist. Deterministic methods, such as the design storm approach, simulate catchment response to

https://doi.org/10.5194/egusphere-2026-2808
Preprint. Discussion started: 11 June 2026

prescribed rainfall events and are more suited to engineering applications but rely on critical assumptions regarding storm duration, shape, and antecedent soil moisture (Camici et al., 2011). Hybrid or derived flood frequency approaches combine both statistical and physical representations. Initially formulated by Eagleson (1972) and further developed by Sivapalan et al. (2005), they link stochastic descriptions of rainfall to rainfall–runoff models to derive the flood frequency curve analytically or through Monte Carlo simulation. These approaches enable a process-based interpretation of flood probabilities, directly connecting storm characteristics, catchment response, and hydrological variability. For example, Viglione et al. (2009) used this approach to examine the effect of event runoff coefficients on the relationship between rainfall and flood return periods. The increasing computational power and availability of stochastic rainfall models have further promoted their application for assessing flood response under climate and land-use change (Rogger et al., 2012; Winter et al., 2019).

The derived flood frequency concept provides an ideal framework for integrating process understanding into flood estimation and for exploring the physical drivers of flood change. In particular, event-based formulations (Ball et al., 2016; Ho et al., 2023) allow the explicit consideration of storm properties and rainfall-runoff interactions, which are both sensitive to climatic drivers. The capacity to model these physical processes makes derived approaches particularly valuable for projecting future flood hazard under non-stationary climate conditions. As pointed out by Merz and Blöschl (2003); Merz et al. (2022), gaining knowledge on the physical mechanisms controlling flood generation is essential for improving predictive reliability, rather than relying solely on statistical distribution approaches. In this study, we build on this concept to explicitly disentangle the effects of individual flood generation mechanisms to analyse how their relative importance and associated flood frequencies are projected to change under future climatic conditions.

Bayesian inference has emerged as a powerful methodological complement to process-based flood analysis. Bayesian frameworks enable the explicit representation of uncertainty in both parameters and model structure, while coherently integrating diverse data sources and prior hydrological knowledge (Ribatet et al., 2007; Kuczera et al., 2010; Renard et al., 2010; Viglione et al., 2013). Within flood frequency analysis, Bayesian methods provide a natural means to link event-scale processes (e.g., rainfall intensity, duration, runoff coefficient, soil moisture) to flood statistics and to propagate uncertainties from climate drivers through to flood quantiles (Meresa et al., 2021; Costa and Fernandes, 2017). Moreover, they allow for hierarchical modeling of catchment similarity and facilitate the pooling of information across regions, enhancing robustness in data-scarce environments.

Despite the progress made in recent decades, most existing studies either assume stationary relationships between rainfall and runoff or treat climatic and hydrological uncertainties independently, thereby limiting their ability to capture the compound effects of changing precipitation and antecedent conditions. While several process-based and stochastic models have been proposed for derived flood frequency analysis, few have explicitly accounted for the seasonal dependence of flood generation mechanisms or their sensitivity to climate forcing. In summary, advancements in flood frequency analysis under climate change can be obtained by: (i) moving beyond stationary statistical formulations; (ii) explicitly incorporating physical processes such as precipitation extremes, antecedent conditions, and rainfall–runoff interactions; (iii) employing Bayesian inference for consistent uncertainty propagation; and (iv) integrating climate model projections to assess the future evolution of flood regimes.

https://doi.org/10.5194/egusphere-2026-2808
Preprint. Discussion started: 11 June 2026

This study presents a Bayesian, climate-sensitive, event-based framework for derived flood frequency analysis calibrated on event characteristics, that explicitly accounts for the seasonal dependence of rainfall–runoff processes and their climate sensitivity. The approach links probabilistic representations of storm, soil moisture, and catchment response through a simple event-based rainfall–runoff model, allowing the joint propagation of uncertainty from climate forcing to flood quantiles. The framework is applied to Austrian hydrological hotspots using long-term records and EURO-CORDEX climate projections, providing a transferable methodology to assess climate-sensitive flood hazards in non-stationary environments. Although the present study focuses on climate-driven changes, the same framework can be readily applied to assess the influence of other drivers of non-stationarity, such as land-use modifications or hydraulic interventions (Hall et al., 2014).

The paper is organized as follows: Section 2 describes the study region. Section 3 outlines the Bayesian stochastic modeling framework and calibration. Section 4 presents the results on process variability, uncertainty decomposition, and projected flood frequency changes. Finally, Section 5 discusses the implications of our findings and Section 6 summarizes key conclusions.

2 Study Region

The study is conducted in Austria, a hydrologically diverse country with complex interactions among topography, climate, geology, and land use. Elevations range from below 200 m in the eastern lowlands to over 3000 m in the western Alps. This topographic gradient drives substantial spatial variability in precipitation, which ranges from less than 400 mm yr^{-1} in the east to nearly 3000 mm yr^{-1} in the mountainous west. Land cover reflects the altitudinal zones: lowlands are predominantly agricultural, mid-elevation regions are forested, and high alpine areas are characterized by sparse vegetation and exposed bedrock. (Merz and Blöschl, 2003; Gaál et al., 2012).

Flood drivers differ across the country. In the western Alps, streamflow is significantly influenced by snow and glacier melt, and most floods occur in summer as a result of frontal systems and, occasionally, convective storms. Snowmelt can enhance antecedent soil moisture conditions, especially for early summer floods. In the southern and southeastern alpine regions, Mediterranean storm tracks cause large autumn floods, while May floods are often dominated by snowmelt. The northern fringe of the Alps experiences high rainfall due to orographic enhancement of northwesterly airflows, with summer floods primarily resulting from prolonged frontal precipitation and minimal snowmelt contribution. In the eastern lowlands, annual precipitation is lower, and floods are generally triggered by frontal and convective events in summer, as well as by rain-on-snow processes in winter. The hilly southeast is particularly prone to short-duration, high-intensity convective storms, which often result in flash flooding in small catchments (Gaál et al., 2012).

To enable a more structured assessment of hydrological response variability, attention was focused on a subset of representative catchment groups, referred to as *hotspots* (Gaál et al., 2012). These are regions in which flood drivers are relatively uniform within the group but differ significantly from other regions. They represent end members along the spectrum of flood process regimes in Austria. Thirteen such hot spots were identified based on hydrological similarity in terms of geology, climate, and runoff behavior. A subset of 10 out of these 13 *hotspots* was considered due to data availability. Each of them contains between two and five catchments, amounting to a total of 38 catchments across all groups. This subdivision enables targeted analysis of

https://doi.org/10.5194/egusphere-2026-2808
Preprint. Discussion started: 11 June 2026

dominant processes within distinct hydrological regimes. Details of the *hotspots* selection procedure are provided in Gaál et al. (2012)

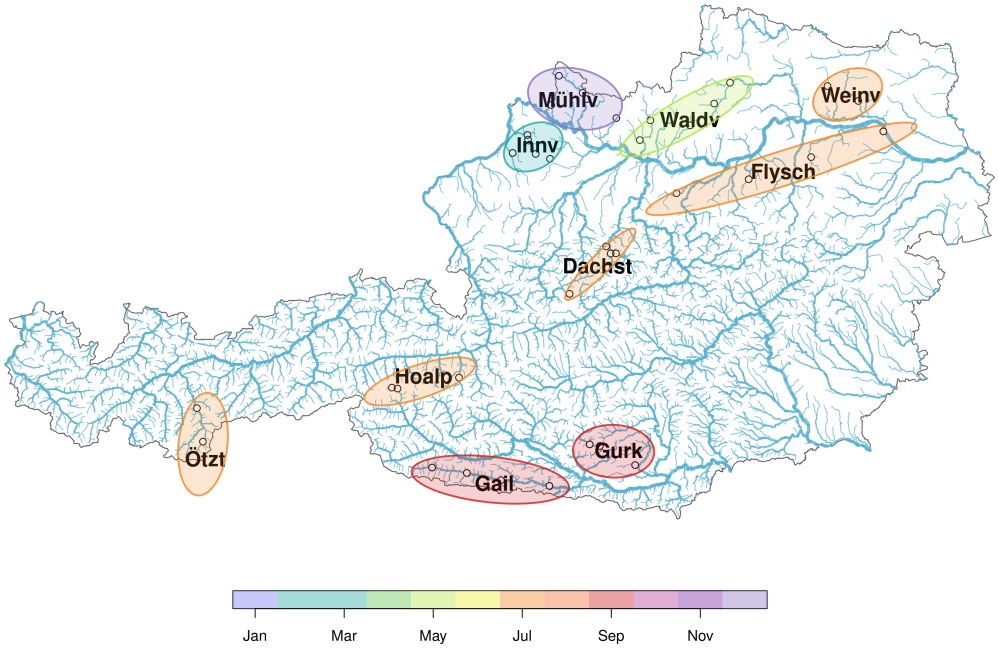

Figure 1. Case study and 10 out of the 13 hotspots identified by Gaál et al. (2012) with flood seasonality. The hotspots were identified based on hydrological similarity in terms of geology, climate, and runoff generation processes.

3 Methodology

The framework is organized into three modules. First, flood events are extracted and characterized from the synthetic hydrometeorological series of the *WETRAX* weather generator, deriving event-scale variables such as storm intensity and duration, liquid precipitation ratio, runoff coefficient, and antecedent catchment conditions. Second, these characteristics are used within a Bayesian stochastic framework to calibrate probabilistic distributions for each process variable; a Monte Carlo simulation then propagates their joint uncertainty through a linear reservoir rainfall–runoff model, yielding empirical flood frequency curves for the present period. Third, parameter changes derived from an ensemble of EURO-CORDEX regional climate projections are introduced to generate future flood frequency curves, and an ANOVA decomposition attributes total uncertainty to model calibration, parameter response, and climate forcing spread.

https://doi.org/10.5194/egusphere-2026-2808
Preprint. Discussion started: 11 June 2026

3.1 Event separation

A robust population of flood events is obtained from the WETRAX+ framework, which integrates a multi-site stochastic weather generator with a distributed rainfall-runoff model. This setup provides spatially and temporally consistent synthetic series of precipitation and air temperature at an hourly resolution, derived from a high-density monitoring network across Austria, Germany, and the Czech Republic. For this study, a 100-year subset of these hourly meteorological data was utilized. These inputs were processed through a distributed rainfall-runoff model, specifically calibrated for the Danube and Drava catchments with an emphasis on high-flow dynamics. This integrated modeling chain ensures a high-resolution characterization of the rainfall-runoff processes, enabling a robust analysis of flood frequency and peak discharges.

The R package `HydroEvents` (Wasko and Guo, 2025) is employed to identify and characterize hydrologically consistent flood events through a sequence of signal-processing procedures. The method starts with the separation of the discharge time series into slow (baseflow) and fast response components, under the assumption that flood events are primarily associated with the latter. Baseflow is separated using the `baseflowA` recursive digital filter, which applies a filter controlled by a recession parameter ($\alpha = 0.999$). The filter is applied iteratively to stabilize the separation and to reduce edge effects, yielding the fast response component of the catchment. Flood events are identified on the fast response component using the `eventMaxima` function, which detects local discharge peaks and evaluates their hydrological relevance based on both magnitude and temporal separation. A Peak-Over-Threshold criterion is adopted, with a seasonal threshold set to the 90th percentile of the fast-flow series, ensuring that only significant runoff responses are retained, and that a sufficient number of events is identified in each season. In addition, a minimum inter-event time of 72 hours is imposed to enforce statistical independence between successive events and to avoid splitting single hydrological responses into multiple artificial events. For each detected peak, the start and end of the runoff event are delineated using custom procedures based on changes in the discharge trend and relative threshold criteria, allowing the extraction of the complete event hydrograph associated with each flood peak. Rainfall events are identified independently using again a Peak-Over-Threshold approach implemented through the `eventMaxima` function. The threshold is defined as the 90th percentile of non-zero precipitation values. Finally, rainfall and runoff events are paired using the `pairEvents` function, which matches events occurring within a physically plausible time window. Event pairing is performed by searching for rainfall events that temporally precede the runoff response, subject to a maximum admissible lag. This lag is defined based on cross-correlation analysis between precipitation and discharge (see Wasko and Guo, 2022, for additional details on the R functions).

The selection of thresholds and parameters involved in event separation and matching was guided by extensive sensitivity testing. Several alternative configurations were explored, varying percentile thresholds, minimum event separation times, and baseflow filter parameters. The final setup was chosen as a compromise that ensured the identification of hydrologically plausible flood events, a consistent temporal correspondence between rainfall and runoff responses, and a sufficient number of events for robust calibration.

For each matched event, a set of key hydrological and meteorological metrics is computed, including event duration, total rainfall, the liquid fraction of precipitation, mean rainfall intensity, runoff volume, fast-response peak flow, peak baseflow, mean

https://doi.org/10.5194/egusphere-2026-2808
Preprint. Discussion started: 11 June 2026

event temperature, mean temperature over the 100 days preceding the event, and cumulative precipitation over the 100 days preceding the event. To overcome the limitations of the standard volumetric ratio method, we estimated the runoff coefficient as an explicit parameter within a simple rainfall-runoff model. Following the approach of Merz and Blöschl (2009), the direct runoff was simulated using a linear reservoir model characterized by a storage parameter and a constant runoff coefficient. The model parameters were calibrated by minimizing the root mean square error between the observed and simulated direct runoff hydrographs. This procedure is significantly less sensitive to the subjective identification of event start and end points (Figure 2), as it accounts for the entire recession limb dynamics.

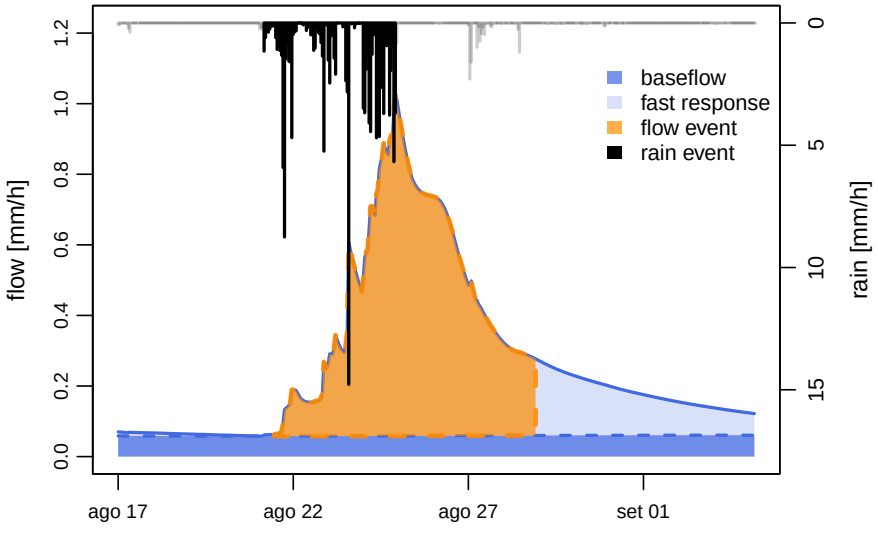

Figure 2. Example of an event identified by the algorithm in an alpine catchment of hotspot 4 (Hochalp)

Once the event characteristics are obtained, to simplify the relationship between the flood peaks and the event-specific flood drivers, the *WETRAX* model is simplified to a linear reservoir rainfall-runoff model, which allows the distinct flood drivers to be isolated and their individual contributions to flood peak magnitude to be quantified. The model represents the catchment response as a standard linear reservoir with response time t_c, through which the rainfall time series is convoluted. For a single storm, the transformation of rainfall to runoff can be expressed by the convolution integral of the exponential unit hydrograph (UH). Assuming rainfall intensity to be constant over the event duration, the peak flood response is:

$$q_p = \Pi_Q(i, t_r, r_c, l_r) = r_c \cdot l_r \cdot i_m \cdot \left[1 - exp\left(-\frac{t_r}{t_c}\right)\right] + q_b \quad (1)$$

where r_c is the event runoff coefficient, l_r the percentage of liquid precipitation, i_m the mean intensity of rainfall, and t_r the event duration.

https://doi.org/10.5194/egusphere-2026-2808
Preprint. Discussion started: 11 June 2026

Figure 3 shows a comparison of flood peaks obtained from the *WETRAX model* and those derived from the simplified linear reservoir model. The latter are obtained by feeding the event characteristics extracted directly into equation (1), thereby reconstructing the flood peak for each identified event. Despite a tendency to overestimate flood peaks in the Weinviertel (Weinv) and Hochalpen (Hoalp) hotspots, the two models show consistently high correlations across all hotspots, suggesting that the linear reservoir captures the relevant flood-generating dynamics. Note that the aim is not to reproduce accurately flood magnitudes, but to isolate the response of flood quantiles to changes in individual climatic drivers.

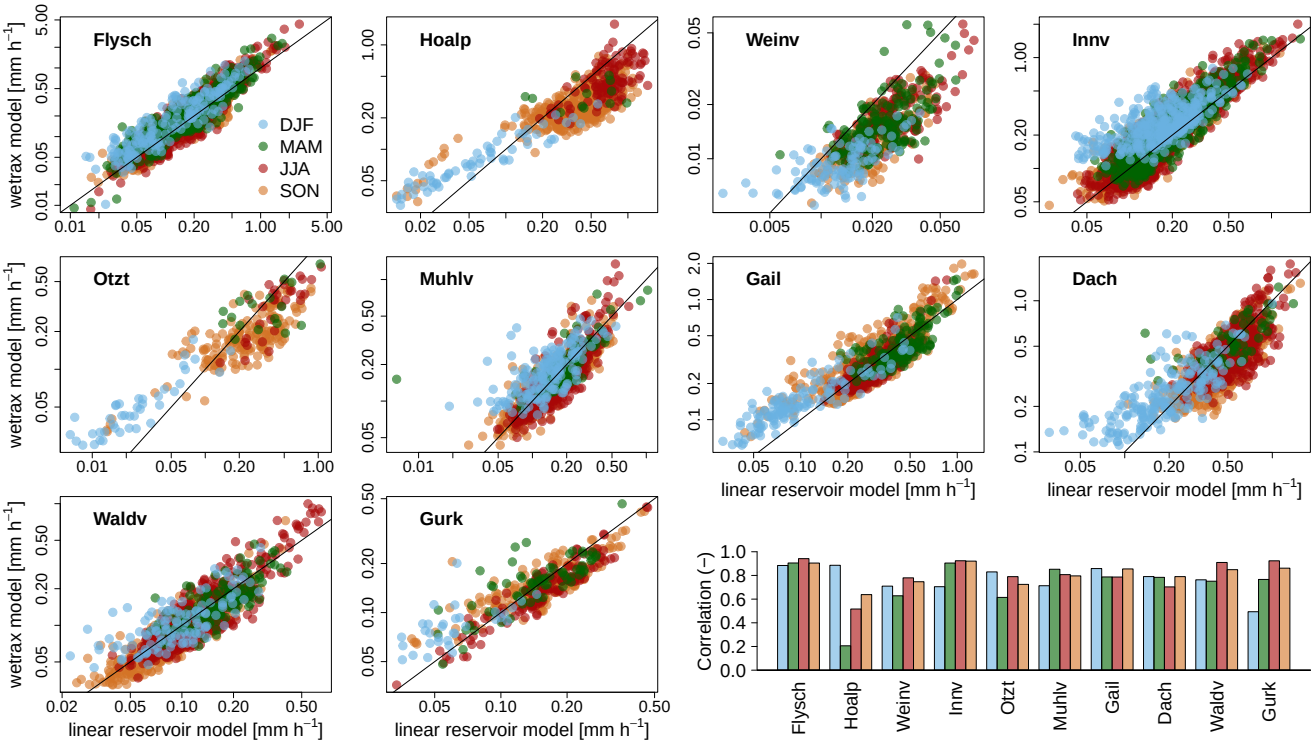

Figure 3. Comparison between flood peaks obtained from the *WETRAX model* and those obtained from the linear reservoir rainfall-runoff model.

3.2 Stochastic model for flood peaks

Aiming at deriving flood frequency curves for varying driver statistics, the methodology builds upon a stochastic representation of event-scale processes, where uncertainty is propagated from climatic inputs (temperature, precipitation) to flood response through probabilistic models.

The derived flood frequency approach is used to estimate "seasonal" flood frequency curves. Essentially, the model consists of discrete rainfall events whose durations, average rainfall intensity, and liquid ratio are all random, governed by specified distributions. A large ensemble of synthetic storm events, reflecting the probabilistic behavior of hydro-meteorological processes,

https://doi.org/10.5194/egusphere-2026-2808
Preprint. Discussion started: 11 June 2026

is simulated using a Monte Carlo approach. The non-exceedence probability of annual flood is estimated by generating a large number of synthetic events, where event runoff coefficient, liquid ratio, storm duration, storm intensity, and baseflow are all random and governed by specified distributions, calibrated on the flood event characteristics identified.

Storm duration and intensity

The event duration t_r is sampled from a 2-parameter Weibull distribution with parameters γ_r (scale) and β_r (shape) (Sivapalan et al., 2005; Viglione and Bloschl, 2009).

$$f_{T_r}(t_r) = \frac{\beta_r}{\gamma_r}\left(\frac{t_r}{\gamma_r}\right)^{\beta_r - 1} \exp\left(-\frac{t_r}{\gamma_r}\right)^{\beta_r} \tag{2}$$

The mean rainfall intensity i_m is sampled as a Gamma distribution (Martinez-Villalobos and Neelin, 2019), whose shape and rate parameters depend on the event duration t_r. The conditional probability density function is defined as:

$$f_{I_m|t_r,}(i_m|t_r) = \frac{\lambda(t_r)}{\Gamma(k(t_r))}\left[\lambda(t_r)\cdot i_m\right]^{k(t_r)-1} \exp\left[-\lambda(t_r)\cdot i_m\right] \tag{3}$$

The shape k and rate λ of the Gamma distribution are related to storm duration as in Sivapalan et al. (2005):

$$\begin{aligned} k(t_r) &= \frac{t_r^{-b_2}}{a_2} \\ \lambda(t_r) &= \frac{t_r^{-b_1-b_2}}{a_1 \cdot a_2} \end{aligned} \tag{4}$$

The conditional moments are:

$$\begin{aligned} \mathbb{E}[i_m \mid t_r] &= a_1 \cdot t_r^{b_1} \\ CV^2[i_m \mid t_r] &= a_2 \cdot t_r^{b_2} \end{aligned} \tag{5}$$

Here, CV^2 denotes the squared coefficient of variation, which quantifies the relative dispersion with respect to the mean.

Liquid ratio

The liquid precipitation ratio l_r accounts for the proportion of total precipitation that occurs in liquid form during a flood-triggering event, excluding the part that falls as snow and thus does not contribute to immediate runoff generation. This factor is sampled using a zero-one inflated Beta distribution (Ospina and Ferrari, 2010), conditional on the event temperature. Specifically, the probability of having fully liquid precipitation ($l_r = 1$) is described by a logistic function of the temperature T:

$$\Pr(l_r = 1 \mid T) = p_1 = \frac{1}{1 + e^{-(\gamma_l \cdot T + \delta_l)}} \tag{6}$$

https://doi.org/10.5194/egusphere-2026-2808
Preprint. Discussion started: 11 June 2026

For events where $0 < l_r < 1$, the variable is assumed to follow a Beta distribution with parameters depending on temperature. The mean μ_{lr} is modeled as a logistic function of temperature, while the precision parameter ϕ_{lr}, which controls the concentration of the distribution around its mean, is modeled exponentially as:

$$\mu_{lr} = \frac{1}{1 + e^{-(\mu_a \cdot T + \mu_b)}}; \quad \phi_{lr} = \exp(\phi_a \cdot T + \phi_b) \tag{7}$$

The shape parameters of the Beta distribution are then given by: $\alpha_{lr} = \mu_{lr} \cdot \phi_{lr}$, and $\beta_{lr} = (1 - \mu_{lr}) \cdot \phi_{lr}$.
This formulation allows the model to account for the spatial variability of precipitation phase across the basin: at higher elevations, solid precipitation is more likely, while at lower elevations, precipitation is predominantly liquid (Allamano et al., 2009). At lower temperatures, the parameter p_1 is small and solid precipitation is likely in a larger portion of the catchment, while at higher temperatures, the likelihood of fully liquid precipitation increases. For partially solid events (i.e., events with both liquid and solid precipitation within the basin), the flexible Beta distribution accommodates the continuous variability in the liquid fraction. The event temperature T is modeled as normally distributed random variables with mean μ_T and standard deviation σ_T.

Runoff coefficient

The event runoff coefficient r_c is treated as a random variable and modeled using the Beta distribution (Gottschalk and Weingartner, 1998). Runoff coefficient depends on volume of rainfall event and initial conditions of the catchment, the more it rains the more the soil is saturated and a soil which was already saturated before the event is more likely to produce larger runoff. For this reason the mean of the runoff coefficient distribution μ_c is modeled considering a dependence on the volume of precipitation, and the wetness index W_{100d}, calculated as the ratio between the cumulated precipitation over the previous 100 days P_{100} and the potential evapotranspiration over the 100 days before the beginning of the flood event. The latter is computed using a modified version of the Blaney–Criddle equation ($ET_p = d\left(-1.55 + 0.96\left(8.128 + 0.457\overline{T}\right)\right) \cdot 100d$). A logistic formulation ensures $\mu_c \in (0, 1)$:

$$\mu_c = \frac{1}{1 + \exp(-\eta \cdot (t_r \cdot i_m) - \zeta \cdot W_{100d} + \lambda)} \tag{8}$$

where the parameters η, ζ, and λ capture the sensitivity of the runoff coefficient to event precipitation, initial catchment conditions, and a baseline offset, respectively. The runoff coefficient is modeled to explicitly account for both the precipitation volume of the ongoing event and the antecedent hydrological state of the catchment represented by W_{100d}. This choice is motivated by evidence showing that runoff coefficients correlate more strongly with indicators of deep soil water storage than with short-term antecedent precipitation indices (Massari et al., 2023). The antecedent temperature T_{100} is modeled as normally distributed random variables with mean $\mu_{T_{100}}$ and standard deviation $\sigma_{T_{100}}$. The cumulative precipitation over the 100 days preceding the event, P_{100}, is modeled as a lognormal random variable, with mean $\mu_{P_{100}}$ and standard deviation $\sigma_{P_{100}}$, reflecting the strictly positive and right-skewed nature of accumulated rainfall amounts. High values of P_{100} are associated with wetter

https://doi.org/10.5194/egusphere-2026-2808
Preprint. Discussion started: 11 June 2026

and less permeable catchment conditions, which tend to increase the runoff coefficient and amplify the flood response to a given storm.

Baseflow

The event-peak baseflow is sampled as a lognormal distribution with mean μ_{bs} and standard deviation σ_{bs}. The dependency of μ_{bs} on precipitation and temperature of the 100 days before the event is given by:

$$\mu_{bs} = \beta_0 + \beta_1 \cdot T_{100d} + \beta_2 \cdot P_{100d} \tag{9}$$

For each simulated season, the number of flood-triggering events N_i is drawn from a Poisson distribution with mean m, representing the expected number of floods occurring in the season (Cupal et al., 2015; Merz et al., 2016). The seasonal maximum peak discharge $q_{\max,i}$ is then recorded as: $q_{\max,i} = \max\{q_1, q_2, \ldots, q_{N_i}\}$. This procedure yields a synthetic time series of 10^6 seasonal maxima, suitable for frequency analysis, allowing to obtain empirical flood frequency curves.

Although the model involves a relatively large number of parameters, this complexity is offset by a major advantage over traditional calibration approaches. Indeed, the model is calibrated on flood event characteristics rather than directly on the peak discharge. This allows the calibration to target the underlying flood-generation mechanisms, improving the ability of the model to reproduce the processes controlling flood formation.

It is worth noting that the event characteristics used for calibration are pooled across all catchments within each hotspot. The primary motivation for this choice is to obtain a substantially larger sample of flood events, which improves the robustness of the Bayesian calibration and reduces parameter uncertainty. The resulting posterior distributions therefore reflect not only the temporal variability of hydro-meteorological processes within individual catchments, but also the spatial variability among catchments belonging to the same group. This is consistent with the regionalization rationale underlying the hotspot definition, which assumes sufficient hydrological similarity within each group to justify the pooling of information.

Table B1 summarizes the choices of likelihoods and priors for each process. The posterior distribution of all parameters was then obtained by combining these prior specifications with the likelihood contributions from the observed data through Bayes' theorem. Sampling from the posterior was performed using Markov Chain Monte Carlo methods (Stan Development Team, 2025), enabling the joint estimation of all parameters and quantification of their uncertainty. Figure 4 shows the fitted probability densities of the hydrometeorological variables entering equation (1), obtained by propagating the posterior parameter distributions through the calibrated stochastic model. Each density curve corresponds to a single draw from the posterior, reflecting the parametric uncertainty in the calibration. The fitted densities are compared against the observed event characteristics extracted from the *WETRAX* model, providing a visual diagnostic of the goodness of fit.

3.3 Propagation of climate change signals

To assess the impacts of climate change, an ensemble of six CORDEX EUR-11 simulations, based on CMIP5 (Jacob et al., 2014; Taylor et al., 2012), is used, with a spatial resolution of 12.5 km, hourly temporal resolution, and scenario RCP 8.5.

https://doi.org/10.5194/egusphere-2026-2808
Preprint. Discussion started: 11 June 2026

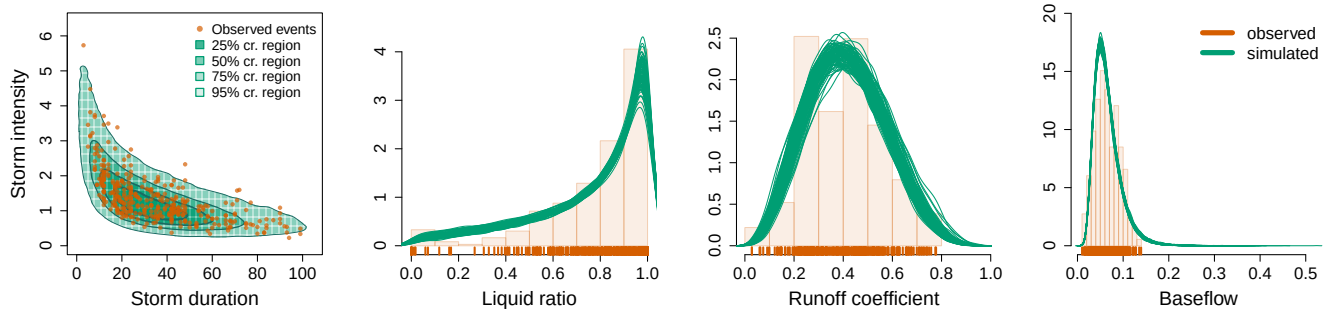

Figure 4. Posterior probability densities of the hydrometeorological variables entering the stochastic flood peak model (equation (1)), compared against the empirical distributions of flood event characteristics extracted from the *WETRAX* model. Each curve represents a density estimate obtained from a single draw of the posterior parameter distribution. Results refer to the autumn season at the Hochalp hotspot.

Two time windows are considered: a control period (1971–2000) and a future period (2071–2100). Precipitation events are extracted from each simulation, and the stochastic model described in Section 3 is calibrated within a unified Bayesian framework, directly inferring probabilistic parameter changes between the reference and future periods. In this way, the model is constrained to incorporate the climate change signal projected by the climate models. Most parameter changes are expressed in relative terms, and therefore no explicit bias-correction procedure is required. For the parameters describing temperature-related distributions, changes are instead represented as absolute differences. This framework allows the impacts of climate change to be characterized in terms of altered precipitation event properties, the expected increase in the liquid fraction of precipitation, changes in the baseflow regime, and modified initial catchment conditions, ultimately leading to different runoff coefficients. Figure 5 illustrates the most relevant process-level variations induced by climate change forcing. The probability density functions are obtained by evaluating the model using the mean values of the fitted parameters.

3.4 Uncertainty decomposition and attribution

To quantify the contribution of different sources of uncertainty in flood frequency estimation under changing climatic conditions, an analysis of variance (ANOVA) was applied to the simulated flood quantiles. Three distinct sources of uncertainty were considered: (i) *calibration uncertainty* (σ^2_c). This component originates from the variability of the posterior parameter distributions obtained during model calibration. It reflects the epistemic uncertainty in estimating the current values of model parameters given the available observations. Each posterior draw represents a plausible model realization under present-day conditions, and the resulting spread in simulated flood quantiles quantifies the uncertainty that would persist even in the absence of climate change. (ii) *parametric response uncertainty* (σ^2_r). This component captures the uncertainty arising from the propagation of parameter changes under future climatic conditions. While the calibration uncertainty describes the lack of knowledge about current parameters, this term accounts for their expected evolution due to altered hydro-climatic regimes, as well as the variability of such changes within each climate model. (iii) *forcing uncertainty* (σ^2_f). The third component arises

https://doi.org/10.5194/egusphere-2026-2808
Preprint. Discussion started: 11 June 2026

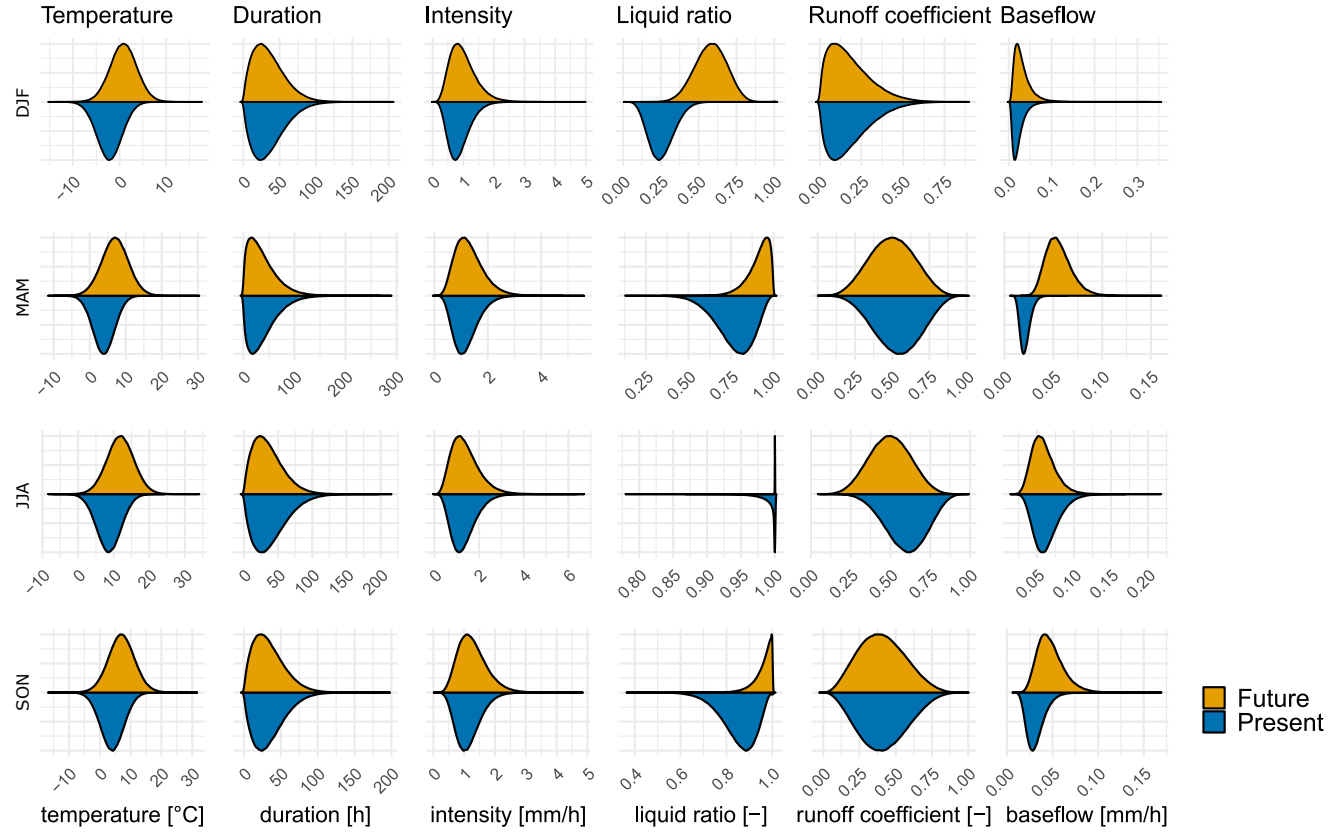

Figure 5. Probability density of the main processes represented in the model and their variation under climate change. The probability density functions are obtained considering the mean values of the fitted parameters. Example shown for the Hochalpen hotspot. The different rows represent different seasons. From top to bottom, winter, spring, summer, and autumn.

from the spread among the different global or regional climate models used as forcing. Each climate model provides distinct climatic trajectories that influence the derived parameter-change distributions.

Let $q_{p,T}$ denote the simulated peak discharge for a given posterior draw p, and return period T for the present period, and $q_{p,m,T}$ for a given posterior draw p, model m, and return period T for the future period. Flood quantiles were organized into a two-dimensional matrix for the present period and a three-dimensional array for future projections, with indices corresponding to posterior draws, return periods, and climate models (only for the future projections). This configuration allows the total variance of projected flood quantiles to be expressed as the sum of three independent components, assuming that uncertainties arising from model calibration, parameter response, and climatic forcing are mutually uncorrelated:

$$\sigma^2{}_{q_T} = \sigma^2{}_{\mathrm{c}} + \sigma^2{}_{\mathrm{r}} + \sigma^2{}_{\mathrm{f}} \tag{10}$$

https://doi.org/10.5194/egusphere-2026-2808
Preprint. Discussion started: 11 June 2026

An ANOVA decomposition on the ensemble of future simulations was used to isolate and normalize each contribution, yielding variance fractions that sum to unity for each return period. To quantify the robustness of projected flood changes, a signal-to-noise ratio (S/N) is computed for each hotspot, season, and return period. The ratio expresses the relative magnitude of the expected mean change in flood quantiles between the future and present periods ($\Delta\mu_{q_T}$) against the standard deviation (σ_{q_T}):

$$\text{S/N} = \frac{|\Delta\mu_{q_T}|}{\sigma_{q_T}} \tag{11}$$

Values of S/N > 1 indicate that the projected flood signal exceeds uncertainty, implying robust detection of change. Conversely, S/N < 1 suggests that uncertainty dominates, and projected changes should be interpreted with caution. This indicator supports the assessment of spatial and seasonal variability in the detectability of flood regime changes across Austria.

4 Results

The seasonal non-exceedance probabilities for each hotspot were estimated following the procedure described in subsection 3.2; see supplementary materials in Cafiero (2026). For the present flood frequency curves, the only source of uncertainty is the *calibration* component, while for future projections, both the *response* and *forcing* components are included. The total uncertainty in the future simulations is therefore substantially larger, reflecting the combined contribution of parameter-response variability and the spread among climate models, in addition to the inherent calibration uncertainty.

The key strength of the proposed framework lies in its ability to disentangle the effects of individual flood drivers, thereby isolating distinct physical drivers of change. Three experimental setups were analyzed: one driven by changes in event temperature, representing the 0°C line shift and its influence on the liquid fraction of precipitation; one capturing the role of antecedent catchment conditions (or soil moisture); and one focusing on variations in precipitation intensity and duration. The combined influence of all mechanisms is represented by the aggregated scenario (`combined`), which integrates the concurrent effects of the three flood generation mechanisms. The projected shifts in the 2-year and 100-year flood quantiles between the present and future periods are illustrated in Figure 6, distinguishing the effects of each driver. Equivalent figures for the remaining hotspots are provided in the Supplementary Material (Cafiero, 2026).

Figure 7 summarizes the expected direction, magnitude, and confidence of the 100-year flood quantile changes across all hotspots and seasons. Triangles indicate whether the change is positive or negative, their size represents the relative magnitude, and their color encodes the robustness of the signal, based on the signal-to-noise ratio (i.e., values > 1 denote high confidence in the direction of change).

To further illustrate the contributions of individual flood drivers, separate maps were produced for each mechanism, showing the projected changes in the 100-year flood quantiles across Austria. The same results obtained for the 2-year flood quantiles are in Appendix A. Figure 8 shows the effect of the temperature-driven shift of the 0°C line, which primarily influences the liquid fraction of precipitation. Figure 9 highlights the role of antecedent catchment conditions, while Figure 10 illustrates the impact of changes in precipitation intensity and duration.

https://doi.org/10.5194/egusphere-2026-2808
Preprint. Discussion started: 11 June 2026

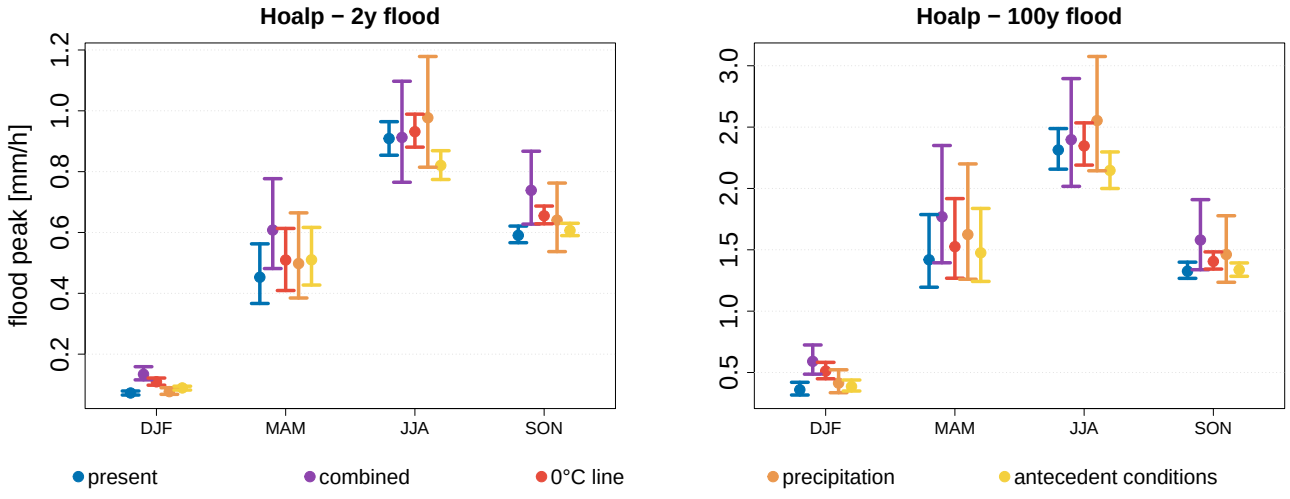

Figure 6. Projected variation of the 2-year (left) and 100-year (right) flood quantile with 80% confidence intervals for the Hochalpen hotspot. Different scenarios isolate the contribution of distinct flood drivers: *0°C line*, capturing the shift of the 0°C isotherm and its influence on the liquid fraction of precipitation; *precipitation*, representing variations in rainfall intensity and duration; and *antecedent conditions*, reflecting changes in soil moisture. The *combined* scenario integrates the concurrent effects of all three mechanisms.

The model is additionally implemented from an annual perspective, complementing the seasonal analysis. In this case as well, the objective is to assess the expected variations in flood quantiles and to disentangle the contributions of different flood drivers to these changes (Figure 11). The annual perspective is particularly relevant because, in several of the cases discussed in the previous figures, the projected increases in flood quantiles do not necessarily occur in the season associated with the largest floods under current conditions. As a result, substantial variations in seasonal flood quantiles do not necessarily translate into variations of annual maxima, and changes in seasonal flood behaviour can alter the relative contribution of different seasons to annual flood extremes. For example, in Alpine hotspots, projections indicate a shift of flood occurrence towards spring, although summer generally remains the season with the largest floods.

Figure 12 illustrates the decomposition of uncertainty sources for the annual configuration of the model, obtained following the methodology described in Section 3.4. The results show that calibration uncertainty contributes a relatively small fraction of the total variance (approximately 5–10%) for return periods up to 100 years. However, its contribution increases markedly for larger return periods, highlighting the growing influence of hydrological parameter uncertainty when simulating extreme flood events. This behavior reflects the enhanced sensitivity of model outputs to parameter values under extreme hydrological conditions. The parametric response uncertainty represents the dominant source of variance across all return periods. This finding indicates that the non-linear propagation of parameter perturbations through the hydrological model plays a key role in shaping the uncertainty of projected flood extremes. Conversely, the contribution of climate forcing uncertainty decreases with increasing return period. Climate model spread has a stronger influence on the variability of more frequent flood events, while its relative influence diminishes for rare extremes.

https://doi.org/10.5194/egusphere-2026-2808
Preprint. Discussion started: 11 June 2026

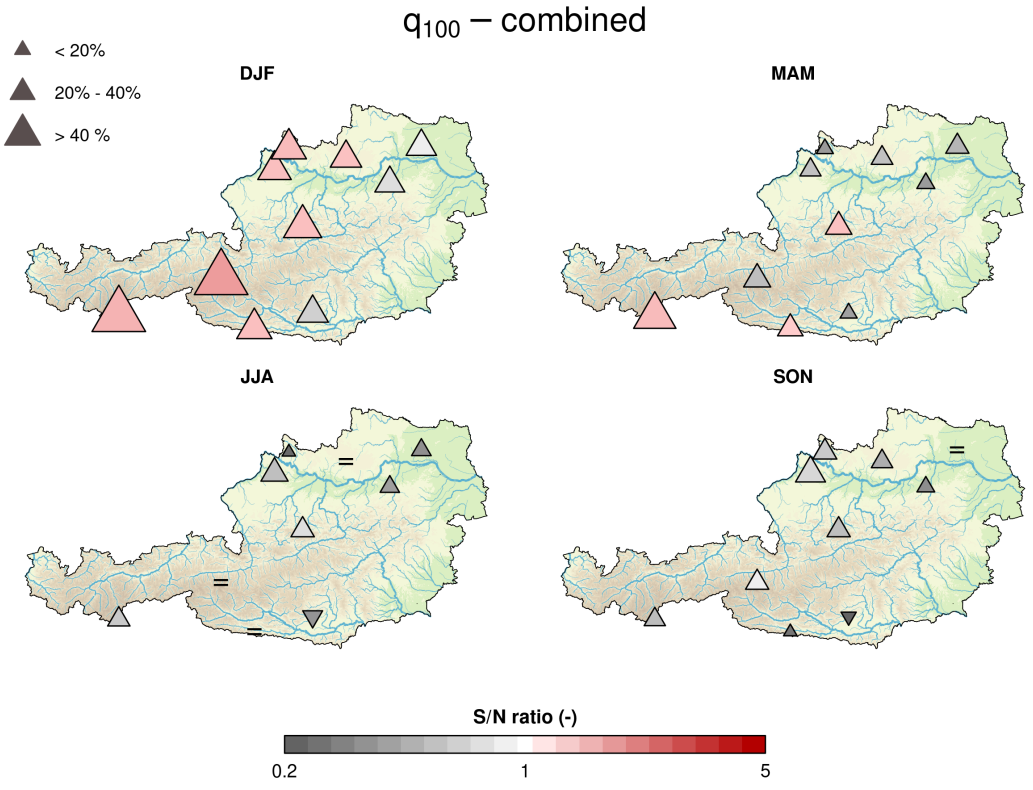

Figure 7. Spatial distribution of projected seasonal 100-year flood changes across Austria. The `combined` scenario integrates the concurrent effects of all three mechanisms. Triangles represent the direction (increase/decrease) and magnitude of the variation, while colors indicate the robustness of the signal, defined by the signal-to-noise ratio (S/N $>$ 1 indicates high confidence). The '=' symbol denotes locations where the projected change ranges between -5% and +5%. River network and elevation data from Copernicus Land Monitoring Service.

5 Discussion

Climate and hydrological processes interact in complex ways to shape flood frequency and magnitude, and their relative importance varies considerably across catchment types and seasons. The modeled responses reflect the combined influence of temperature, precipitation, and antecedent catchment conditions, whose contributions need to be disentangled to interpret the regional differences emerging from the results. Understanding which flood drivers dominate under different climatic regimes is therefore key to assessing future flood hazard and identifying the main sources of uncertainty in the projections.

Overall, the results indicate that changes in precipitation intensity emerge as the primary driver of projected variations in flood frequency and magnitude across the analyzed catchments. At the same time, precipitation projections are characterized by the largest source of uncertainty, reflecting both model spread and the inherent variability of extreme rainfall under climate change. In contrast, temperature-driven processes and antecedent catchment conditions, such as soil moisture and snow dynamics, generally exert a more moderate influence on flood quantile variations at the regional scale. However, their effects tend to be

https://doi.org/10.5194/egusphere-2026-2808
Preprint. Discussion started: 11 June 2026

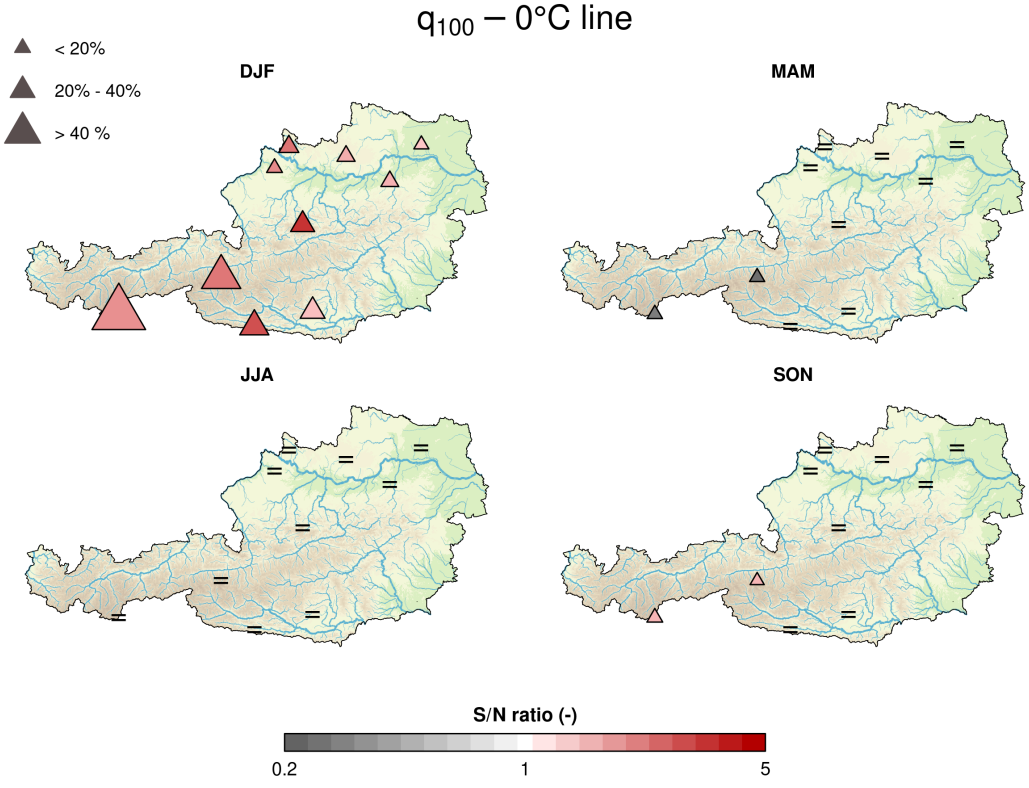

Figure 8. Spatial distribution of projected seasonal 100-year flood changes due to the upward shift of the 0°C line across Austria. Triangles represent the direction (increase/decrease) and magnitude of the variation, while colors indicate the robustness of the signal, defined by the signal-to-noise ratio (S/N $>$ 1 indicates high confidence). The '=' symbol denotes locations where the projected change ranges between -5% and +5%. River network and elevation data from Copernicus Land Monitoring Service.

more systematic and therefore easier to anticipate, as they are governed by comparatively robust physical mechanisms and exhibit lower inter-model variability. This highlights a trade-off between impact and predictability: the processes with the strongest influence on future floods are also those characterized by the highest uncertainty, while secondary drivers contribute more modestly but in a more consistent and interpretable manner.

The relative importance of these processes further depends on the type of flood event considered. As suggested by previous studies, antecedent catchment conditions play a particularly relevant role in shaping more frequent, moderate floods, while precipitation extremes increasingly dominate the generation of rare events (Macdonald et al., 2024). Our results strongly confirm this hypothesis: the influence of antecedent conditions is significantly more pronounced for the 2-year flood than for the 100-year flood. Conversely, the relative impact of precipitation intensity on more frequent floods is comparatively smaller than on rare events. Regarding the upward shift of the 0°C isotherm and the resulting change in the partitioning between solid and liquid precipitation, this effect is clearly visible during the winter season across the whole of Austria. Notably, this

https://doi.org/10.5194/egusphere-2026-2808
Preprint. Discussion started: 11 June 2026

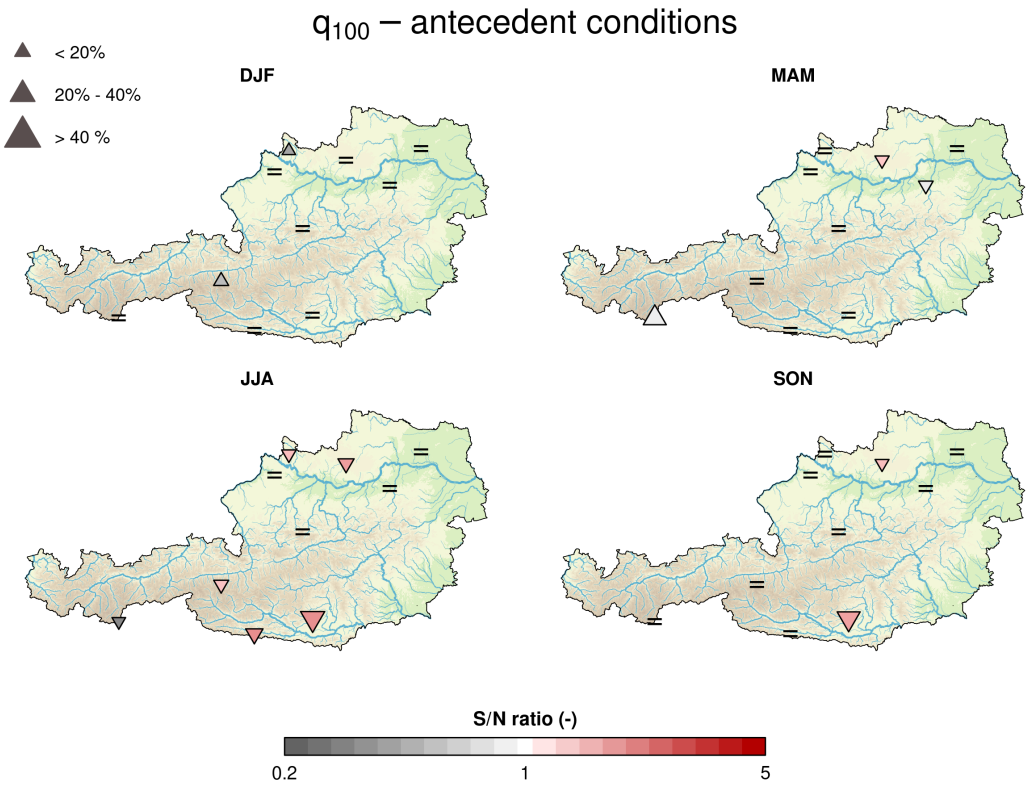

Figure 9. Spatial distribution of projected seasonal 100-year flood changes due to the variation of soil moisture across Austria. Triangles represent the direction (increase/decrease) and magnitude of the variation, while colors indicate the robustness of the signal, defined by the signal-to-noise ratio (S/N $>$ 1 indicates high confidence). The '=' symbol denotes locations where the projected change ranges between -5% and +5%. River network and elevation data from Copernicus Land Monitoring Service.

mechanism affects the 2-year flood much more than the 100-year flood. However, since this increase occurs during a season characterized by minor flood events, the shift in the 0°C line does not significantly influence flood frequency when analyzed on an annual scale. Another widespread pattern concerns the summer season, where a distinct decrease in flood magnitudes is observed when isolating the effect of soil moisture variations, reflecting the impact of increased evapotranspiration and drier initial conditions under a warming climate.

A distinct pattern emerges in Alpine hotspots, characterized by strong seasonal dynamics. First, there is a substantial percentage increase in winter floods; however, these remain minor in absolute terms when compared to summer floods. This winter trend is almost entirely driven by the upward shift of the 0°C isotherm, which increases the liquid fraction of precipitation. Second, during the spring, all three analyzed mechanisms vary in phase, collectively contributing to a rise in flood magnitudes. This is particularly evident for more frequent floods, where the combined signal is most robust. Third, the summer season is characterized by a clear trade-off between competing drivers: while projected increases in precipitation intensity tend to increase

https://doi.org/10.5194/egusphere-2026-2808
Preprint. Discussion started: 11 June 2026

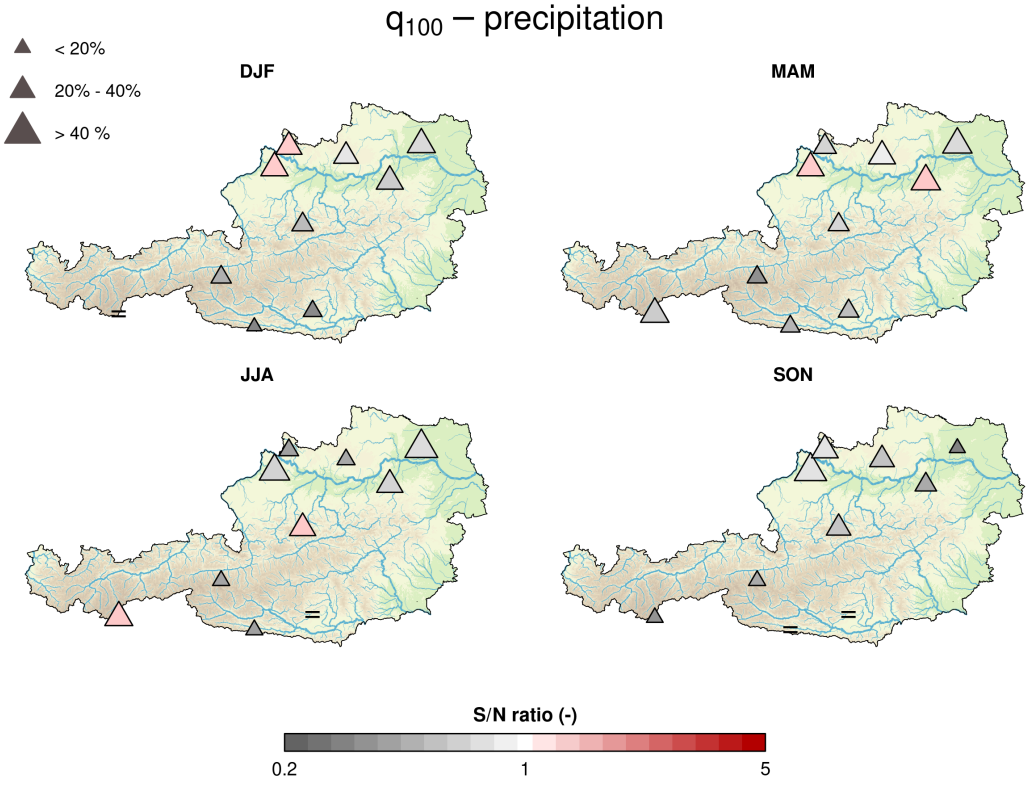

Figure 10. Spatial distribution of projected 100-year flood changes due to precipitation extremes variation across Austria, shown for each season. Triangles represent the direction (increase/decrease) and magnitude of the variation, while colors indicate the robustness of the signal, defined by the signal-to-noise ratio (S/N $>$ 1 indicates high confidence). The '=' symbol denotes locations where the projected change ranges between -5% and +5%. River network and elevation data from Copernicus Land Monitoring Service.

flood magnitudes, this signal is largely uncertain. Conversely, the reduction in available soil moisture decreases flood peaks (especially for more frequent floods). Consequently, ordinary floods are projected to experience a slight, uncertain decrease, while rare floods show a slight, uncertain increase. Fourth, the expected flood variation in autumn is largely dominated by the variation in precipitation intensity. Unlike the summer season, where dry soils act as a significant modulator, the intensification of autumn rainfall translates more directly into increased discharge.

Similar patterns in terms of flood variation were reported by Laaha et al. (2025), who analyzed trends in mean annual flood in Austria for the period 1977–2020. While their study focuses on observed trends in the recent past and the present analysis addresses expected future variations, this comparison provides a consistency check to assess whether projected changes align with recent hydrological behaviour. In particular, they found an increase in winter floods, especially in the southern part of the country. For the spring season, a comparable pattern is observed: flood magnitudes increase in the Alpine region, whereas no clear signal is evident north of the Alps.

https://doi.org/10.5194/egusphere-2026-2808
Preprint. Discussion started: 11 June 2026

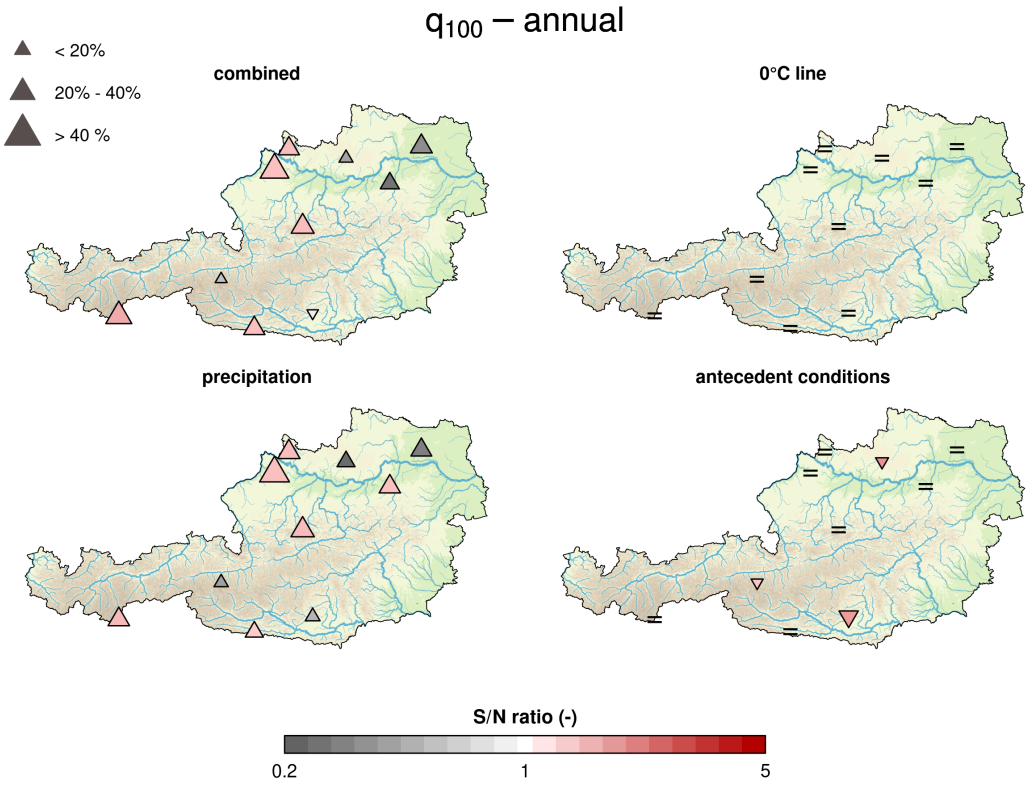

Figure 11. Spatial distribution of projected annual 100-year flood changes caused by different flood generation mechanisms variation across Austria. Triangles represent the direction (increase/decrease) and magnitude of the variation, while colors indicate the robustness of the signal, defined by the signal-to-noise ratio (S/N >1 indicates high confidence). The '=' symbol denotes locations where the projected change ranges between -5% and +5%. River network and elevation data from Copernicus Land Monitoring Service.

The uncertainty analysis reveals that the majority of projected flood variations are accompanied by substantial noise components, reflecting large contributions from both parameter-response and climate-forcing uncertainty, which respectively represent the uncertainty arising from the propagation of parameter changes under future climate conditions, and the one arising from the distinct climate trajectories provided by each member of the ensemble of climate models. On the other hand, Calibration uncertainty, reflecting the epistemic uncertainty in estimating the current values of model parameters, remains consistently minor. This indicates that the robustness of flood projections depends primarily on how model parameters respond to climatic perturbations, and on the variability among climate models, rather than model calibration.

Overall, the linear reservoir model performs acceptably in representing the flood peaks of the distributed model, given the trade-off between simplicity and accuracy. However, flood peaks tend to be overestimated in the Weinv hotspot and underestimated in the alpine hotspots during winter. Moreover, the number of flood-generating events per season was assumed to remain stationary between historical and future periods. This assumption was required because climate model outputs only provide

https://doi.org/10.5194/egusphere-2026-2808
Preprint. Discussion started: 11 June 2026

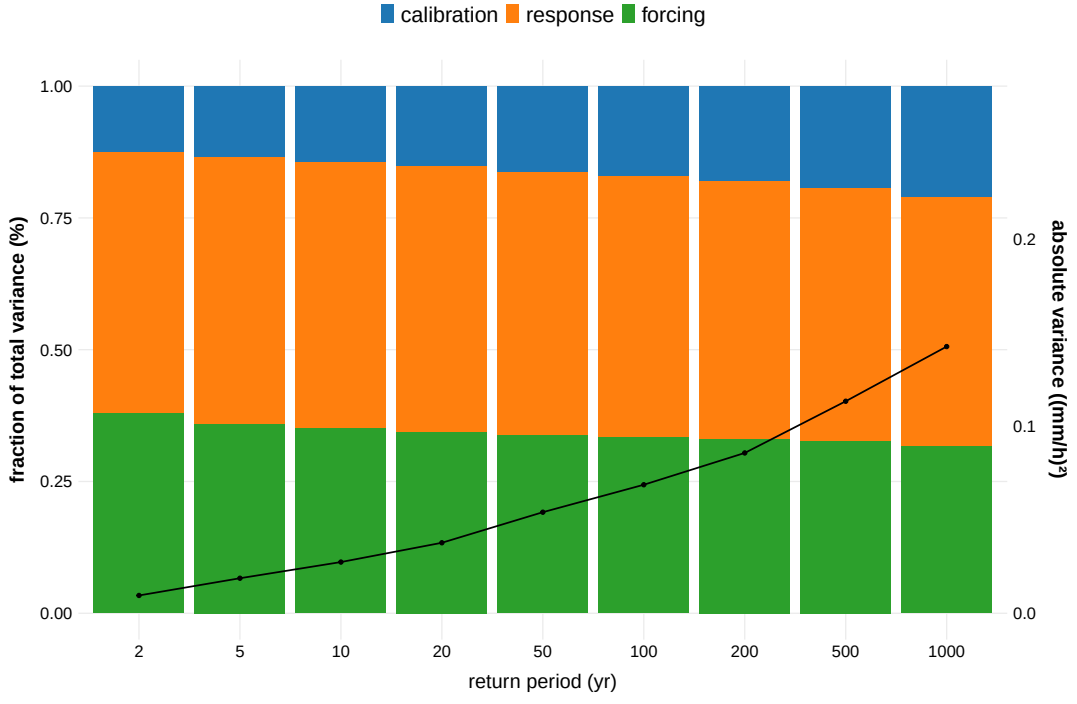

Figure 12. Fractional contribution of each uncertainty source to total flood quantile variance under future climate scenarios. Calibration uncertainty (blue) represents the epistemic uncertainty in estimating current values of model parameters. Response uncertainty (orange) reflects the uncertainty arising from the propagation of parameter changes under future climatic conditions. Forcing uncertainty (green) corresponds to the spread among forcing models. Black lines represent the absolute variance, highlighting the strong increase in uncertainty with larger return periods. These values are obtained by averaging the different uncertainty sources for all the hotspots.

precipitation, while runoff is not directly simulated. Since flood events were identified from discharge series, potential changes in their frequency cannot be inferred directly from climate model output and are therefore not considered in this analysis. To assess the sensitivity of the results to this assumption, additional simulations were performed by perturbing the mean number of flood-generating events per season m by $\pm 20\%$. As expected, increasing m amplifies projected flood quantile changes when the signal indicates an increase, while decreasing m dampens it, and vice versa for negative signals. However, these perturbations do not qualitatively alter the main conclusions of the analysis. Future work should focus on explicitly representing such changes. It should also be noted that the reported variations in flood frequency refer solely to climatic influences; catchment-related effects and river engineering structures were not considered in the evaluation of future flood frequency changes (Blöschl et al., 2007). Nevertheless, Bertola et al. (2019) analyzed the impacts of these different types of changes in Upper Austria, finding that atmospheric drivers, particularly short-duration extreme precipitation, exert a stronger influence on flood frequency variations than catchment or river-scale modifications.

https://doi.org/10.5194/egusphere-2026-2808
Preprint. Discussion started: 11 June 2026

6 Conclusions

This study presents a process-based framework to assess the impact of climate change on flood frequency, explicitly accounting for different sources of uncertainty and the response of key hydrological processes. By integrating a Bayesian event-based model with regional climate projections, the approach allows disentangling the contributions of temperature shifts, antecedent soil moisture, and precipitation intensity to future flood behavior. The framework is applied in Austria, where results indicate that projected changes in flood quantiles highly depend on season and location. In particular, summer floods exhibit a complex trade-off between increasing precipitation intensity and decreasing soil moisture, while winter floods, especially in alpine areas, are particularly sensitive to the increased liquid fraction of precipitation during the event. Moreover, shifts in flood seasonality may alter the relative contribution of individual seasons to annual extremes, highlighting the importance of considering both seasonal and annual perspectives. Overall, these results emphasize that reliable projections of flood frequency under climate change depend on the accurate representation of process responsiveness, particularly the nonlinear propagation of precipitation and temperature effects through catchment hydrology. This methodology provides a transparent and flexible tool for attributing and quantifying drivers of change in flood risk under a warming climate, offering valuable insights for adaptation planning and hydrological modeling under uncertainty.

Code and data availability. The flood event characteristics and the RStan code used for model calibration are available on Zenodo (Cafiero, 2026).

Appendix A

This appendix presents the same results shown in the main text, but focusing on floods with a 2-year return period instead of the 100-year return period, providing a complementary perspective on flood changes across Austria under future climate conditions.

https://doi.org/10.5194/egusphere-2026-2808
Preprint. Discussion started: 11 June 2026

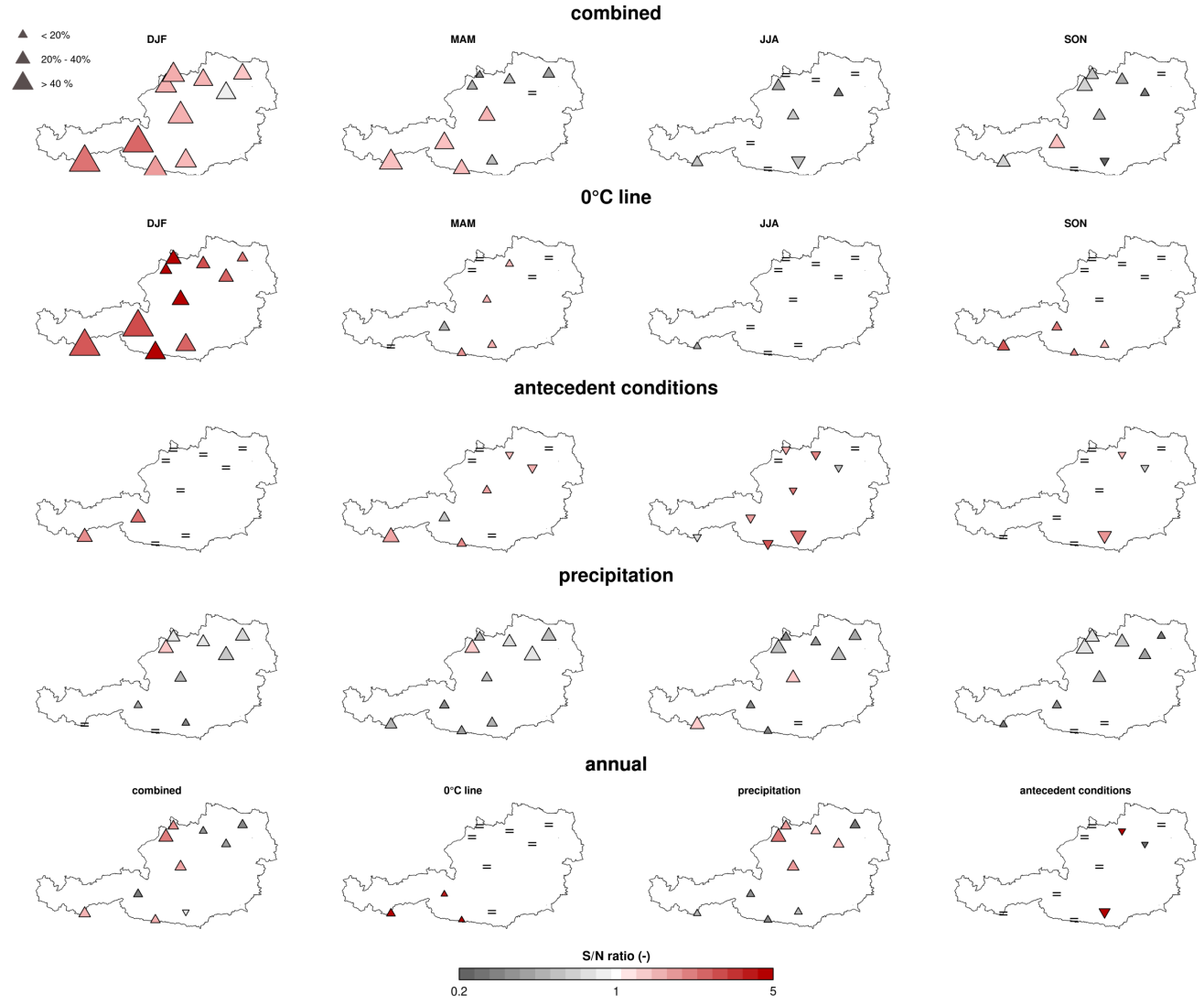

Figure A1. Spatial distribution of seasonal (rows 1-4) and annual (row 5) projected 2-year flood changes across Austria. Arrows represent the direction (increase/decrease) and magnitude of the variation, while colors indicate the robustness of the signal, defined by the signal-to-noise ratio (S/N $>$ 1 indicates high confidence).

https://doi.org/10.5194/egusphere-2026-2808
Preprint. Discussion started: 11 June 2026

Appendix B

Table B1. Summary of likelihoods and priors for each process in the Bayesian model. Likelihoods are chosen to reflect the physical domain and stochastic behavior of each process variable. Distribution choices were based on Sivapalan et al. (2005); Westra et al. (2014); Gottschalk and Weingartner (1998); Viglione et al. (2009)

Process	Likelihood	Parameters	Priors
Event duration	$t_r \sim \text{Weibull}(\beta_r, \gamma_r)$	β_r, γ_r	$\beta_r \sim \text{Gamma}(2,1)$; $\log \gamma_r \sim \text{Normal}(4,1)_{>0}$
Event mean intensity	$i \sim \text{Gamma}(\kappa, \lambda)$	a_1, a_2, b_1, b_2	$a_1 \sim \text{Normal}(5,3)_{>0}$; $a_2 \sim \text{Normal}(0.3, 0.2)$; $b_1 \sim \text{Normal}(0,2)_{<0}$; $b_2 \sim \text{Normal}(0,2)$
Runoff coefficient	$rc \sim \text{Beta}(\mu_c, \phi_c)$	$\eta, \zeta, \lambda, \phi_c$	$\eta, \zeta \sim \text{Normal}(0,1)_{>0}$; $\lambda \sim \text{Normal}(0,2)$; $\phi_c \sim \text{Normal}(30,20)_{>0}$
Liquid ratio	$l_r \sim p_1 \cdot \delta(1) + (1-p_1) \cdot \text{Beta}(\alpha_{lr}, \beta_{lr})$, $p_1 = \text{logistic}(\gamma_l \cdot T + \delta_l)$, $\mu_{lr} = \text{logistic}(\mu_a \cdot T + \mu_b)$, $\phi_{lr} = \exp(\phi_a \cdot T + \phi_b)$	$\mu_a, \mu_b, \phi_a, \phi_b, \gamma_l, \delta_l$	All $\sim \text{Normal}(0,5)$
Event temperature	$temp \sim \text{Normal}(\mu_T, \sigma_T)$	μ_T, σ_T	$\mu_T \sim \text{Normal}(0,20)$; $\sigma_T \sim \text{Cauchy}(0,5)_{>0}$
Precipitation 100 days	$P_{100d} \sim \text{Lognormal}(\mu_{P_{100}}, \sigma_{P_{100}})$	$\mu_{P_{100}}, \sigma_{P_{100}}$	$\mu_{P_{100}} \sim \text{Normal}(0,5)$; $\sigma_{P_{100}} \sim \text{Cauchy}(0,2)_{>0}$
Temperature 100 days	$T_{100d} \sim \text{Normal}(\mu_{T_{100}}, \sigma_{T_{100}})$	$\mu_{T_{100}}, \sigma_{T_{100}}$	$\mu_{T_{100}} \sim \text{Normal}(0,20)$; $\sigma_{T_{100}} \sim \text{Cauchy}(0,5)_{>0}$
Baseflow	$B \sim \text{Lognormal}(\mu, \sigma_B)$, $\mu = \beta_0 + \beta_1 T_{\text{obs}} + \beta_2 P_{\text{obs}}$	$\beta_0, \beta_1, \beta_2, \sigma_B$	$\beta_0 \sim \text{Normal}(0,10)$; $\beta_1, \beta_2 \sim \text{Normal}(0,1)$; $\sigma_B \sim \text{Normal}(0,1)$

Author contributions. **Luigi Cafiero:** Conceptualization, Data Curation, Formal Analysis, Methodology. **Miriam Bertola:** Conceptualization, Writing – review and editing. **Peter Valent:** Data Curation. **Francesco Laio:** Writing – review and editing. **Günter Blöschl:** Writing – review and editing.**Alberto Viglione:** Supervision, Conceptualization, Methodology, Writing – review and editing.

https://doi.org/10.5194/egusphere-2026-2808
Preprint. Discussion started: 11 June 2026

Competing interests. The authors declare that they have no conflict of interest.

Acknowledgements. This study received funding from the Italian Ministry of University and Research (PRIN project n. 2022AX3882 - Clim2FlEx - Mapping of climate to flood extremes).

https://doi.org/10.5194/egusphere-2026-2808
Preprint. Discussion started: 11 June 2026

References

Allamano, P., Claps, P., and Laio, F.: Global warming increases flood risk in mountainous areas, Geophysical Research Letters, 36, https://doi.org/https://doi.org/10.1029/2009GL041395, 2009.

Ball, J., Babister, M., Nathan, R., Weinmann, P., Weeks, W., Retallick, M., and Testoni, I.: Australian Rainfall and Runoff-A guide to flood estimation, 2016.

Bennett, B., Leonard, M., Deng, Y., and Westra, S.: An empirical investigation into the effect of antecedent precipitation on flood volume, Journal of Hydrology, 567, 435–445, https://doi.org/https://doi.org/10.1016/j.jhydrol.2018.10.025, 2018.

Bertola, M., Viglione, A., and Blöschl, G.: Informed attribution of flood changes to decadal variation of atmospheric, catchment and river drivers in Upper Austria, Journal of Hydrology, 577, 123 919, https://doi.org/https://doi.org/10.1016/j.jhydrol.2019.123919, 2019.

Bertola, M., Viglione, A., Vorogushyn, S., Lun, D., Merz, B., and Blöschl, G.: Do small and large floods have the same drivers of change? A regional attribution analysis in Europe, Hydrology and Earth System Sciences, 25, 1347–1364, https://doi.org/10.5194/hess-25-1347-2021, 2021.

Blöschl, G., Ardoin-Bardin, S., Bonell, M., Dorninger, M., Goodrich, D., Gutknecht, D., Matamoros, D., Merz, B., Shand, P., and Szolgay, J.: At what scales do climate variability and land cover change impact on flooding and low flows?, Hydrological Processes, 21, 1241–1247, https://doi.org/https://doi.org/10.1002/hyp.6669, 2007.

Blöschl, G., Hall, J., Viglione, A., Parajka, H. S., Merz, M. B., Sivapalan, S., Smith, R. A., and Bates, P. A.: Changing climate both increases and decreases European river floods, Nature, 573, 108–111, https://doi.org/10.1038/s41586-019-1495-6, 2019.

Cafiero, L.: Supplementary material – Climate-sensitive Derived Flood Frequency Analysis Based on Flood Events Characteristics, https://doi.org/10.5281/zenodo.20051452, [data set], 2026.

Camici, S., Tarpanelli, A., Brocca, L., Melone, F., and Moramarco, T.: Design soil moisture estimation by comparing continuous and storm-based rainfall-runoff modeling, Water Resources Research, 47, 2011.

Camici, S., Brocca, L., Melone, F., and Moramarco, T.: Impact of Climate Change on Flood Frequency Using Different Climate Models and Downscaling Approaches, Journal of Hydrologic Engineering, 19, 04014 002, https://doi.org/10.1061/(ASCE)HE.1943-5584.0000959, 2014.

Costa, V. and Fernandes, W.: Bayesian estimation of extreme flood quantiles using a rainfall-runoff model and a stochastic daily rainfall generator, Journal of Hydrology, 554, 137–154, https://doi.org/https://doi.org/10.1016/j.jhydrol.2017.09.003, 2017.

Cupal, M., Deev, O., and Linnertova, D.: The Poisson Regression Analysis for Occurrence of Floods, Procedia Economics and Finance, 23, 1499–1502, https://doi.org/https://doi.org/10.1016/S2212-5671(15)00465-7, 2nd GLOBAL CONFERENCE on BUSINESS, ECONOMICS, MANAGEMENT and TOURISM, 2015.

Eagleson, P. S.: Dynamics of flood frequency, Water Resources Research, 8, 878–898, https://doi.org/10.1029/WR008i004p00878, 1972.

Estilow, T. W., Young, A. H., and Robinson, D. A.: A long-term Northern Hemisphere snow cover extent data record for climate studies and monitoring, Earth System Science Data, 7, 137–142, https://doi.org/10.5194/essd-7-137-2015, 2015.

Gaál, L., Szolgay, J., Kohnová, S., Parajka, J., Merz, R., Viglione, A., and Blöschl, G.: Flood timescales: Understanding the interplay of climate and catchment processes through comparative hydrology, Water Resources Research, 48, https://doi.org/https://doi.org/10.1029/2011WR011509, 2012.

Gottschalk, L. and Weingartner, R.: Distribution of peak flow derived from a distribution of rainfall volume and runoff coefficient, and a unit hydrograph, Journal of hydrology, 208, 148–162, 1998.

https://doi.org/10.5194/egusphere-2026-2808
Preprint. Discussion started: 11 June 2026

Hall, J., Arheimer, B., Borga, M., Brázdil, R., Claps, P., Kiss, A., Kjeldsen, T. R., Kriaučiūnienė, J., Kundzewicz, Z. W., Lang, M., Llasat, M. C., Macdonald, N., McIntyre, N., Mediero, L., Merz, B., Merz, R., Molnar, P., Montanari, A., Neuhold, C., Parajka, J., Perdigão, R. A. P., Plavcová, L., Rogger, M., Salinas, J. L., Sauquet, E., Schär, C., Szolgay, J., Viglione, A., and Blöschl, G.: Understanding flood regime changes in Europe: a state-of-the-art assessment, Hydrology and Earth System Sciences, 18, 2735–2772, https://doi.org/10.5194/hess-18-2735-2014, 2014.

Haslinger, K., Breinl, K., Pavlin, L., Pistotnik, G., Bertola, M., Olefs, M., Greilinger, M., Schöner, W., and Blöschl, G.: Increasing hourly heavy rainfall in Austria reflected in flood changes, Nature, 639, 667–672, https://doi.org/10.1038/s41586-025-08647-2, 2025.

Ho, M., Wasko, C., O'Shea, D., Nathan, R., Vogel, E., and Sharma, A.: Changes in flood-associated rainfall losses under climate change, Journal of Hydrology, 625, 129 950, https://doi.org/https://doi.org/10.1016/j.jhydrol.2023.129950, 2023.

Jacob, D., Petersen, J., Eggert, B., Alias, A., Christensen, O., Bouwer, L., Braun, A., Colette, A., Déqué, M., Georgievski, G., Georgopoulou, E., Gobiet, A., Menut, L., Nikulin, G., Haensler, A., Hempelmann, N., Jones, C., Keuler, K., Kovats, S., and Yiou, P.: EURO-CORDEX: New high-resolution climate change projections for European impact research, Regional Environmental Change, 14, https://doi.org/10.1007/s10113-013-0499-2, 2014.

Kemter, M., Merz, B., Marwan, N., Vorogushyn, S., and Blöschl, G.: Joint Trends in Flood Magnitudes and Spatial Extents Across Europe, Geophysical Research Letters, 47, e2020GL087 464, https://doi.org/https://doi.org/10.1029/2020GL087464, e2020GL087464 2020GL087464, 2020.

Kuczera, G., Renard, B., Thyer, M., and Kavetski, D.: There are no hydrological monsters, just models and observations with large uncertainties!, Hydrological Sciences Journal, 55, 980–991, https://doi.org/10.1080/02626667.2010.504677, 2010.

Laaha, G., Laimighofer, J., Parajka, J., Bertola, M., and Blöschl, G.: Abflusstrends in Österreichs Fließgewässern 1977–2020, Österreichische Wasser- und Abfallwirtschaft, 77, 338–346, https://doi.org/10.1007/s00506-024-01106-8, 2025.

Macdonald, E., Merz, B., Guse, B., Nguyen, V. D., Guan, X., and Vorogushyn, S.: What controls the tail behaviour of flood series: rainfall or runoff generation?, Hydrology and Earth System Sciences, 28, 833–850, https://doi.org/10.5194/hess-28-833-2024, 2024.

Madsen, H., Lawrence, D., Lang, M., Martinkova, M., and Kjeldsen, T.: Review of trend analysis and climate change projections of extreme precipitation and floods in Europe, Journal of Hydrology, 519, 3634–3650, https://doi.org/https://doi.org/10.1016/j.jhydrol.2014.11.003, 2014.

Martinez-Villalobos, C. and Neelin, J. D.: Why Do Precipitation Intensities Tend to Follow Gamma Distributions?, Journal of the Atmospheric Sciences, 76, 3611 – 3631, https://doi.org/10.1175/JAS-D-18-0343.1, 2019.

Massari, C., Pellet, V., Tramblay, Y., Crow, W. T., Gründemann, G. J., Hascoetf, T., Penna, D., Modanesi, S., Brocca, L., Camici, S., and Marra, F.: On the relation between antecedent basin conditions and runoff coefficient for European floods, Journal of Hydrology, 625, 130 012, https://doi.org/https://doi.org/10.1016/j.jhydrol.2023.130012, 2023.

Meresa, H., Murphy, C., Fealy, R., and Golian, S.: Uncertainties and their interaction in flood hazard assessment with climate change, Hydrology and Earth System Sciences, 25, 5237–5257, https://doi.org/10.5194/hess-25-5237-2021, 2021.

Merz, B., Nguyen, V. D., and Vorogushyn, S.: Temporal clustering of floods in Germany: Do flood-rich and flood-poor periods exist?, Journal of Hydrology, 541, 824–838, https://doi.org/https://doi.org/10.1016/j.jhydrol.2016.07.041, 2016.

Merz, B., Basso, S., Fischer, S., Lun, D., Blöschl, G., Merz, R., Guse, B., Viglione, A., Vorogushyn, S., Macdonald, E., Wietzke, L., and Schumann, A.: Understanding Heavy Tails of Flood Peak Distributions, Water Resources Research, 58, e2021WR030 506, https://doi.org/https://doi.org/10.1029/2021WR030506, e2021WR030506 2021WR030506, 2022.

https://doi.org/10.5194/egusphere-2026-2808
Preprint. Discussion started: 11 June 2026

Merz, R. and Blöschl, G.: A process typology of regional floods, Water Resources Research, 39, https://doi.org/https://doi.org/10.1029/2002WR001952, 2003.

Merz, R. and Blöschl, G.: Flood frequency hydrology: 1. Temporal, spatial, and causal expansion of information, Water Resources Research, 44, https://doi.org/https://doi.org/10.1029/2007WR006744, 2008.

Merz, R. and Blöschl, G.: A regional analysis of event runoff coefficients with respect to climate and catchment characteristics in Austria, Water Resources Research, 45, https://doi.org/https://doi.org/10.1029/2008WR007163, 2009.

Ospina, R. and Ferrari, S. L. P.: Inflated beta distributions, Stat. Pap., 51, 111–126, https://doi.org/10.1007/s00362-008-0125-4, 2010.

Renard, B., Kavetski, D., Kuczera, G., Thyer, M., and Franks, S. W.: Understanding predictive uncertainty in hydrologic modeling: The challenge of identifying input and structural errors, Water Resources Research, 46, https://doi.org/https://doi.org/10.1029/2009WR008328, 2010.

Ribatet, M., Sauquet, E., Gresillon, J. M., and Ouarda, T. B. M. J.: A regional Bayesian POT model for flood frequency analysis, Stochastic Environmental Research and Risk Assessment, 21, 327–339, https://doi.org/10.1007/s00477-006-0069-9, 2007.

Rogger, M., Kohl, B., Pirkl, H., Viglione, A., Komma, J., Kirnbauer, R., Merz, R., and Blöschl, G.: Runoff models and flood frequency statistics for design flood estimation in Austria – Do they tell a consistent story?, Journal of Hydrology, 456-457, 30–43, https://doi.org/https://doi.org/10.1016/j.jhydrol.2012.05.068, 2012.

Sivapalan, M., Blöschl, G., Merz, R., and Gutknecht, D.: Linking flood frequency to long-term water balance: Incorporating effects of seasonality, Water Resources Research, 41, https://doi.org/10.1029/2004WR003439, 2005.

Stan Development Team: RStan: the R interface to Stan, https://mc-stan.org/, r package version 2.32.7, 2025.

Taylor, K. E., Stouffer, R. J., and Meehl, G. A.: An Overview of CMIP5 and the Experiment Design, Bulletin of the American Meteorological Society, 93, 485 – 498, https://doi.org/https://doi.org/10.1175/BAMS-D-11-00094.1, 2012.

Viglione, A. and Bloschl, G.: On the role of storm duration in the mapping of rainfall to flood return periods, Hydrology and Earth System Sciences, 13, 205–216, https://doi.org/10.5194/hess-13-205-2009, 2009.

Viglione, A., Merz, R., and Blöschl, G.: On the role of the runoff coefficient in the mapping of rainfall to flood return periods, Hydrology and Earth System Sciences, 13, 577–593, https://doi.org/10.5194/hess-13-577-2009, 2009.

Viglione, A., Merz, R., Salinas, J. L., and Blöschl, G.: Flood frequency hydrology: 3. A Bayesian analysis, Water Resources Research, 49, 675–692, https://doi.org/10.1002/wrcr.20079, 2013.

Wasko, C. and Guo, D.: Understanding event runoff coefficient variability across Australia using the hydroEvents R package, Hydrological Processes, 36, https://doi.org/10.1002/hyp.14563, 2022.

Wasko, C. and Guo, D.: hydroEvents: Extract Event Statistics in Hydrologic Time Series, https://CRAN.R-project.org/package=hydroEvents, r package version 0.12.0, 2025.

Wasko, C., Nathan, R., Stein, L., and O'Shea, D.: Evidence of shorter more extreme rainfalls and increased flood variability under climate change, Journal of Hydrology, 603, 126 994, https://doi.org/https://doi.org/10.1016/j.jhydrol.2021.126994, 2021.

Westra, S., Fowler, H. J., Evans, J. P., Alexander, L. V., Berg, P., Johnson, F., Kendon, E. J., Lenderink, G., and Roberts, N. M.: Future changes to the intensity and frequency of short-duration extreme rainfall, Reviews of Geophysics, 52, 522–555, https://doi.org/10.1002/2014RG000464, 2014.

Winter, B., Schneeberger, K., Dung, N., Huttenlau, M., Achleitner, S., Stötter, J., Merz, B., and Vorogushyn, S.: A continuous modelling approach for design flood estimation on sub-daily time scale, Hydrological Sciences Journal, 64, 539–554, https://doi.org/10.1080/02626667.2019.1593419, 2019.